Effects of Mantle Flow on Hotspot Motion

Bernhard Steinberger

Institut für Meteorologie und Geophysik, Johann Wolfgang Goethe-Universität, Frankfurt am Main, Germany

Richard J. O'Connell

Department of Earth and Planetary Sciences, Harvard University, Cambridge, Massachusetts

The motion of hotspots in large–scale mantle flow is discussed. The concept of mantle plumes and the experiments and observations on which it is based are reviewed. Results that support hotspot motion (from experiments, plate reconstructions and paleolatitude data) are contrasted with observations on which the concept of hotspot fixity is based (mainly geometry and age progression of hotspot tracks). A numerical model of hotspot motion in large-scale mantle flow is introduced. It is shown how hotspot motion may approximately represent flow at mid–mantle depth, particularly plate return flow. Such a model can explain some aspects of the observed hotspot distribution, yields predictions on the origin and shape of plume conduits and gives constraints on mantle viscosity structure. Some results for the motion of individual hotspots are shown, including coherent motion toward the southeast for Hawaii and Louisville, westward motion for Easter, and southward motion for Kerguelen. For Hawaii and Louisville, the calculated motion fits well the observed geometry and age progression of hotspot tracks. Furthermore, calculations can explain observed relative motions of Pacific and African hotspots back to 43 Ma without invoking any additional plate boundary in the Pacific-Antarctic region. Paleomagnetic and modelling results of polar motion are reviewed and combined with models of hotspot motion; resulting predictions of paleolatitudes are compared with observations for the Pacific plate. Calculated hotspot motion in combination with polar motion can explain any latitudinal shift of Pacific hotspots back to about 70-80 Ma.

1. INTRODUCTION

Hotspots have long been regarded as fixed and are therefore used as reference points for plate motion. Nevertheless, hotspot motion is expected from dynamical mantle flow models. There is as well observational evidence for hotspot motion. In this paper, we review arguments for and against hotspot motion, with emphasis on a qualitative discussion of the behavior of plume conduits in mantle flow in section 3. We then introduce our numerical model of plumes in mantle flow. This model was developed in order to contribute to the discussion about hotspot motion from a geodynamic perspective. Our results are in accordance with predictions arising

The History and Dynamics of Global Plate Motions
Geophysical Monograph 121

from the qualitative discussion. Our proposed model includes moderate motion of hotspots as well as polar motion and reconciles many observations.

2. EXPERIMENTAL AND OBSERVATIONAL EVIDENCE FOR MANTLE PLUMES

We begin by reviewing experiments and observations that support the existence of mantle plumes: Since the groundbreaking works of *Wilson* [1963], *Morgan* [1971,1972] and others it has been recognized that hotspots are caused by sources of heat – presumably upwellings from deep in the mantle – that are essentially stationary i.e. they move much more slowly than the tectonic plates. This insight was mainly based on the observation that active hotspot volcanoes are frequently associated with chains of islands and seamounts that get older with increasing distance from the active hotspot and that the age progressions can often be explained by a rigid plate moving over fixed hotspots. As an example, Figure 1 shows topography and age progression of the Reunion hotspot track on the African and Indian plate. This hotspot simultaneously left tracks on both plates for a period of time, while it presumably was close to the plate boundary. The age progression is different on both plates, as the plates moved at different speed relative to the hotspot.

Subsequent laboratory experiments showed that "If the upwelling material has less viscosity than the surrounding material, the structure ... eventually ascends as a spherical pocket of fluid fed by a pipe" [*Whitehead and Luther,* 1975]. This kind of upwelling became the standard model of a "mantle plume"; examples are shown in Figure 2. The exact shape and development of plumes depends on the viscosity contrast inside and outside the plume, whether the plume continues to be fed from the boundary layer, and to what extent material of the surrounding mantle is entrained. Detailed treatments are given by *Olson and Singer* [1985] and *Griffiths and Campbell* [1990]. When scaled to Earth dimensions, the experiments suggest a plumehead radius of a few hundred km, whereas the trailing conduit has a radius of a few tens of km at most; the ascent time of the plumehead through the mantle is of the order of 100 Ma, with large uncertainties. Obviously, the experiments are a simplification of plumes in the real Earth, which are expected to rise from the time-dependent boundary layer of a system convecting at high Rayleigh number. Nevertheless, the concept that plumeheads in the mantle establish rather narrow conduits is widely accepted. Those conduits may subsequently be affected by large-scale flow, as detailed in the next section.

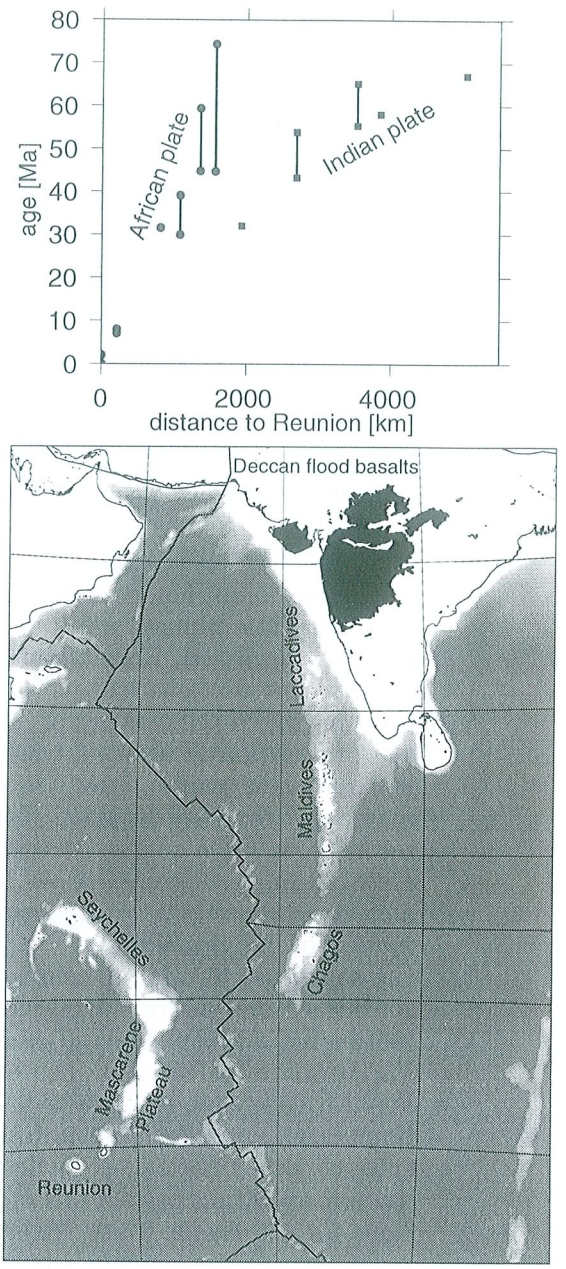

Figure 1. The Reunion hotspot track. The distribution of Tertiary extrusives in India (Deccan traps) is shown in black, according to *Choubert and Faure-Muret* [1976]. Topography is shown in greyshades between -3000 and -1000 m, in white above -1000 m, and in uniform grey below -3000 m. This figure and all other maps were made using GMT graphics [*Wessel and Smith,* 1995], with topography from ETOPO5 data [*National Geophys. Data Center,* 1988]. Age data of sea floor basalts along the track (shown as circles for African plate, squares for Indian plate) are from *Duncan and Hargraves* [1990] and references herein, and compiled by *Müller et al.* [1993].

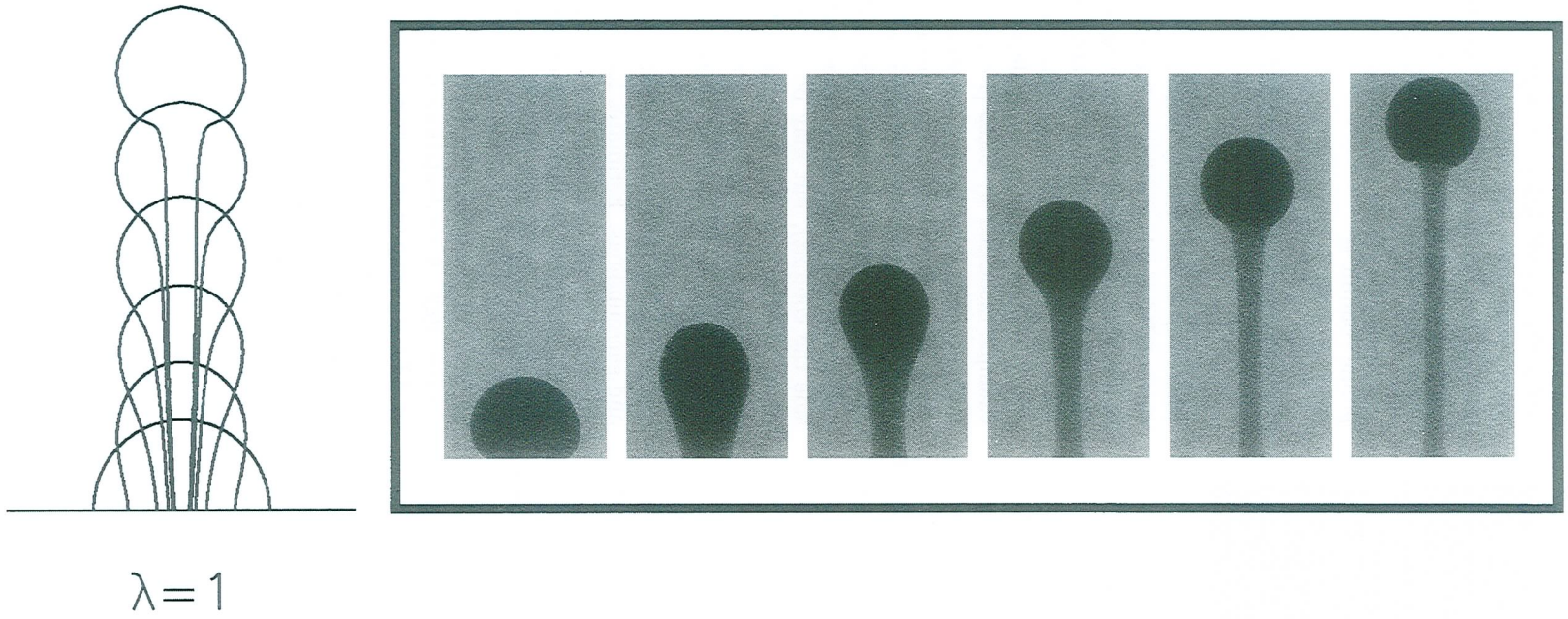

Figure 2. Experimental and numerical realization of a plume; figures are reproduced from *Manga et al.* [1993]. These results were obtained for a constant volume plume and the same viscosity η inside and outside the conduit at low Reynolds number. Total time of the experiment is $42\eta/(\Delta\rho g r)$, where $\Delta\rho$ is density contrast, g is gravity, r is plumehead radius. This can be readily scaled to parameters expected for the Earth's mantle. Results look similar for constant feeding rate, except that the plumehead grows with time [*Olson and Singer,* 1985; *Griffiths and Campbell,* 1990], hence its rise speed will not approach a limit; the ratio of conduit to head diameter becomes smaller as the ratio of viscosity inside to outside the conduit decreases [*Whitehead and Luther,* 1975].

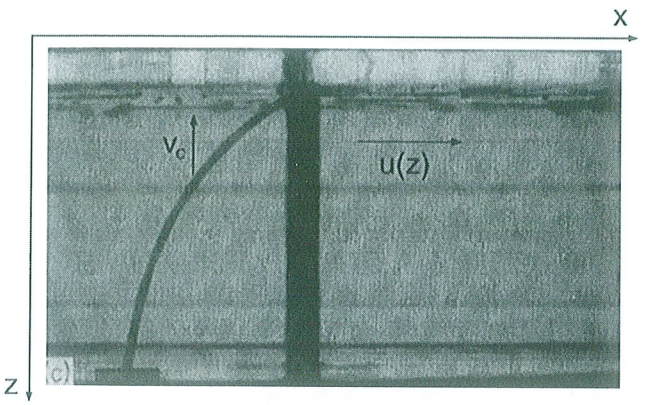

Figure 3. Experimental realization of a plume tilted in large-scale flow. Figure after *Richards and Griffiths* [1988].

The notion that plumes consist of "heads" and "tails" (conduits) is also supported by observations: Many plume tracks – corresponding to the motion of a plate over the tail – begin with extensive flood basalts – corresponding to the eruption of the plumehead. The clearest example is the association of the Deccan flood basalts with the Reunion hotspot track (Figure 1). The subject is discussed more extensively by *Richards et al.* [1989].

3. DISTORTION OF A PLUME CONDUIT IN SHEAR FLOW

Richards and Griffiths [1988] simulated the tilt of a plume in a simple experiment (Figure 3): The plume conduit is advected (horizontally) in large-scale flow (here: horizontal flow speed $u(z)$), but conduit elements also rise buoyantly (here: buoyant "Stokes" rising speed v_c of the conduit through the surrounding viscous mantle – which is not to be confused with the rising speed of material through the conduit); total velocity of each conduit element is simply the vector sum of ambient flow velocity $\mathbf{u}$ and rising velocity $\mathbf{v}_c$. In the case of this experiment (stationary, fixed plume source; horizontal simple shear flow; constant viscosity of fluid outside conduit) a parabolic conduit shape results, as can be seen. The situation in the real Earth is more complicated: the source of the conduit is not fixed in space, but moves with the flow; mantle flow is not only horizontal; buoyant rising speed varies with depth; plumes are probably thermal features such that there is no sharp distinction between plume and surroundings. Nevertheless, the simple concept that motion of each conduit element can be calculated as vector sum $\mathbf{u} + \mathbf{v}_c$ may still be approximately valid for the Earth and is therefore used in our models.

Based on this simple concept we will now qualitatively discuss the behavior of hotspot plumes in large-scale mantle flow, beginning with the variables that determine v_c. The same effects as discussed here will also appear in our numerical model. Ambient mantle flow $\mathbf{u}$ will be further discussed in section 6.

A modified Stokes' formula for the rising speed of a plume conduit is

$$v_c = \frac{0.54 \Delta\rho g r_c^2}{\eta_{out}}, \tag{1}$$

where $\Delta\rho$ is the density contrast between plume and surroundings, g is gravity, r_c is conduit radius and η_{out} is the viscosity of the surrounding mantle. Obviously this equation is a rather crude approximation: Neither the effects of boundaries (surface and CMB) and viscosity interfaces nor any time dependence (such as for example discussed by *Sleep* [1992]) are considered. A more accurate treatment is however also prevented since many of the model parameters are not well constrained.

The numerical value 0.54 has been determined experimentally by *Richards and Griffiths* [1988] for a "chemical" plume (i.e. with different materials inside and outside the conduit), but may be different for a thermal plume conduit, which is not materially distinct from the surrounding mantle and hence may also rise by thermal entrainment of surrounding mantle [*Richards and Griffiths,* 1989].

$\Delta\rho$ is due to the temperature contrast between plume and surroundings. Estimates for plume excess temperature ΔT are of the order 200 to 300 K [e.g., *Schilling,* 1991]. For representative values ΔT = 300 K, thermal expansivity $\alpha = 3 \cdot 10^{-5}\mathrm{K}^{-1}$ and mantle density $\rho_m = 3300\mathrm{kg\ m}^{-3}$ we obtain $\Delta\rho = 30\mathrm{kg\ m}^{-3}$. Whereas ρ_m and ΔT increase with depth (see *Albers and Christensen* [1996] for calculations of the depth dependence of ΔT), α is expected to decrease to values of less than $10^{-5}K^{-1}$ in the lower part of the lower mantle [*Chopelas and Boehler,* 1989], where therefore somewhat smaller values of $\Delta\rho$ are expected.

η_{out} is usually inferred from models of postglacial rebound and the geoid. None of these methods can constrain details of mantle viscosity structure so that considerable uncertainties remain. Models of postglacial rebound give some kind of viscosity "average" for about the upper half of the mantle, with resolving power decreasing with depth. This "average" was determined to 10^{21} Pas in the classic paper by *Haskell* [1935], and a recent re-analysis by *Mitrovica* [1996] obtains a similar result. Some depth dependence can also be resolved,

with results indicating a substantial increase of viscosity with depth [*Mitrovica*, 1996; *Lambeck and Johnston*, 1998]. For example, the preferred viscosity structure of *Lambeck and Johnston* [1998] features an increase from $4 \cdot 10^{20}$ Pas above the transition zone to 10^{22} Pas or greater in the lower mantle. Models of the geoid based on mantle density heterogeneities in a dynamic Earth were developed by *Ricard et al.* [1984] and *Richards and Hager* [1984]. They do not constrain absolute viscosity, but also show an increase of viscosity with depth. The limitations of this method have been discussed by *Thoraval and Richards* [1997], indicating that a robust feature of many models again is a substantial viscosity increase with depth (at least a factor of 30). A joint model of postglacial rebound and the geoid by *Mitrovica and Forte* [1997], also indicates a similar viscosity increase. The viscosity structure used here in most cases ($4 \cdot 10^{20}$ Pas between 100 and 400 km, 10^{21} Pas in the transition zone, and an increase in the lower mantle in four steps of 200 km from 10^{22} Pas to a maximum value of $4 \cdot 10^{22}$ Pas below 1270 km and above D", i.e. a viscosity increase with depth by a factor 100, henceforth referred to as "viscosity model A") is in accordance with the evidence cited above, however our models of hotspot motion favor an even stronger viscosity increase [*Steinberger and O'Connell*, 1998], and we will also show some results for the preferred viscosity structure of that paper (here referred to as "viscosity model B"). Similar to the approach presented here, a high-viscosity lower mantle has been previously inferred from models of hotspot motion [*Richards*, 1991].

r_c can be estimated from scaling laboratory experiments to Earth dimensions to be a few tens of km or less (as mentioned above). Similar values in the upper mantle can also be inferred from the width of most hotspot tracks (of the order of 100 km or less) and associated gravity anomalies [e.g., *Morgan*, 1972]. r_c might be somewhat larger in the lower mantle, as will be argued below. Also the fact that most hotspot plumes have not been observed by seismic tomography indicates narrow conduits. Seismic observations have been reported for the Iceland plume, indicating $r_c \sim 150$ km in the upper mantle [*Wolfe et al.*, 1997] and $r_c < 250$ km in the lower mantle [*Bijwaard and Spakman*, 1999], however this might be broader than usual, as this is the first tomographic evidence reported for a whole mantle plume.

Another estimate of r_c can be made from Poiseuille's formula for flow in a pipe, which can be written

$$r_c = \left(\frac{8 B \eta_{in}}{\pi \Delta\rho dp/dz} \right)^{\frac{1}{4}} \qquad (2)$$

where B is the anomalous mass flux of the plume conduit (defined as volume flux times difference of density inside and outside the conduit), η_{in} is the viscosity inside the conduit and dp/dz is the non-hydrostatic pressure gradient driving flow through the conduit. η_{in} and dp/dz are not well constrained, but at least eqn. 2 indicates how r_c is expected to vary with anomalous mass flux and depth, and it gives an estimate in accordance with the above:

The anomalous mass flux B has been determined for various hotspots based on the magnitudes of associated topographic swells [*Davies*, 1988; *Sleep*, 1990]. For plumes close to ridges, the length of the geochemical anomaly gives an additional constraint [*Schilling*, 1991]. Results indicate anomalous mass fluxes between about $0.3 \cdot 10^3$ kg/s for the smallest plumes and $8 \cdot 10^3$ kg/s for the largest one (Hawaii). Differences between various estimates are considerable, with uncertainties largest for the smallest hotspots.

Because of the higher temperature, η_{in} is expected to be considerably less than η_{out}. If the temperature is adiabatic both inside and outside the conduit, the ratio η_{in}/η_{out} may be constant, but due to thermal entrainment, η_{in}/η_{out} is expected to increase with decreasing depth. Taking $\eta_{in} = 10^{19}$ Pas as a reasonable guess, and using the hydrostatic approximation $dp/dz = \Delta\rho g$ with $\Delta\rho = 30$ kg m^{-3} as estimated above, we get $r_c \approx 40$ km for a representative value $B = 10^3$ kg/s, resp. $r_c \approx 70$ km for the Hawaiian plume flux $B = 8.3 \cdot 10^3$ kg/s (Table 1), in accordance with the above estimates. The actual value of dp/dz might be considerably smaller [*Sleep*, 1992], but η_{in} might also be smaller. Conduits of the largest plumes should be about a factor $(8/0.3)^{1/4} \sim 2$ thicker than for the smallest plumes, and for a viscosity increase of a factor 100, r_c will increase with depth by a factor $(100)^{1/4} \sim 3$ or less.

In the upper mantle, the observed sharpness of the bend in the Hawaiian-Emperor-Chain gives an important constraint on the rising speed. As pointed out by *Griffiths and Richards* [1989], the deflection of the Hawaiian plume in the uppermost mantle (a layer of low viscosity below the lithosphere) is likely not more than 200 km. The reason is also explained in Figure 4. Using numerical values for plate motion $u_0 \approx 10$ cm/yr and a layer thickness of $d \approx 300$ km (estimated thickness of the mantle layer of lowest viscosity, as discussed above), this implies a rising speed of at least about 7.5 cm/yr, and correspondingly less for smaller plumes. In any case, a few cm/yr is probably a reasonable estimate for a conduit rising speed in the uppermost viscosity layer, corresponding to a horizontal deflection of typically a few hundred km or less and a typical risetime of the

Table 1. Parameters used for the hotspots shown. Ages are equal to age of associated flood basalt, where available (Tristan, Reunion, Kerguelen, Louisville), otherwise inferred from the length of the track (Samoa, Tahiti), or reasonable guesses are made, where the end of the track has been subducted (Hawaii, Easter). Anomalous mass fluxes B are based on *Davies* [1988], *Sleep* [1990], *Schilling* [1991] and *Davies* [1992].

Hotspot	Age, Ma	$B[10^3 \mathrm{kg/s}]$
Easter	100, 60	2.1
Hawaii	100	8.3
Kerguelen	117	0.9
Louisville	120	3.0
Reunion	67	1.4
Samoa	14	1.6
Tahiti	5	4.5
Tristan	125	1.0

conduit of the order of 10 Ma or less. For comparison, with the above estimates $r_c = 70$ km, $\Delta\rho = 30\mathrm{kg\ m}^{-3}$ and $\eta_{out} = 4 \cdot 10^{20}$ Pas, eqn. 1 gives $v_c \approx 6$ cm/yr for the Hawaiian plume in the upper mantle. This shows that the above estimates are almost in accordance, but rising speed cannot be lower than estimated above (such as would be the case for a significantly thinner conduit).

Although Figure 4, which reiterates the argument made by *Griffiths and Richards* [1989], is a simplification, it summarizes the effects that we expect flow in the "low-viscosity" uppermost mantle to have on conduit shape and hotspot motion. We can classify three possible kinds of behavior (although in reality they will not be sharply distinct):

1. As the plumehead presumably rises comparatively fast, it will establish a conduit that is closer to vertical. In an initial stage (lasting a time equal to the rise time of the conduit through the layer of low viscosity, about 10 Ma or less) the conduit will get tilted, and the hotspot will move (a few 100 km, at most) in the direction of the plate, until the shape remains stationary

2. If the plate changes its motion, the conduit will adjust its shape, and the hotspot will move in the direction of the difference of plate motions before and after the change (again, a few 100 km at most, lasting about 10 Ma or less).

3. During other times, the conduit shape will remain stationary in the uppermost mantle. The observed length of hotspot tracks indicates typical hotspot lifetimes of $t_l = 100$Ma or more, and plate reconstructions show that plate motions also tend to remain constant over long periods of time, such that we expect this to be the usual case. In the simple case shown in Figure 4, this would correspond to a fixed hotspot. More realistically, the exit point of the plume from the lower mantle will also move, and the hotspot surface motion will approximately represent the motion of this point; the stationary shape corresponds to the conduit shown in Figure 3, with the difference that the plume source moves in our model.

Motion of that exit point (which is probably not sharply defined in the Earth as viscosity increase with depth may be gradual, but nevertheless provides a useful concept) may be due to two reasons: Firstly, it is due

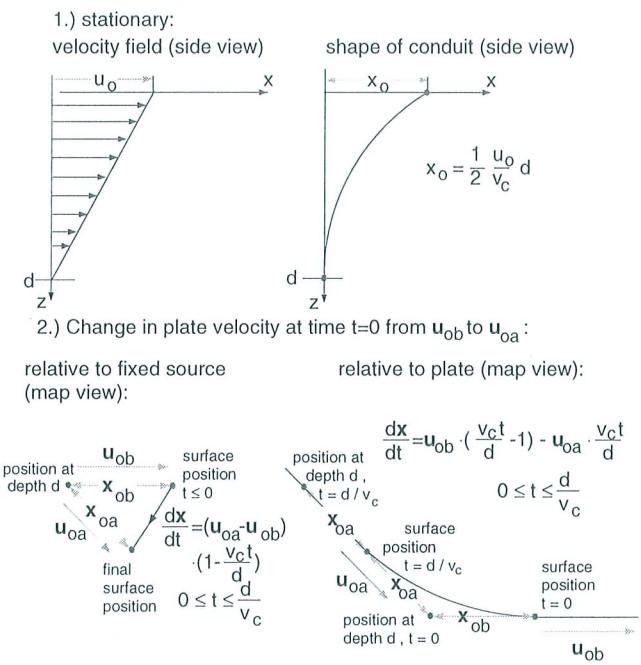

Figure 4. Plumes deflection in the upper mantle and curvature of hotspot track for change in plate velocity – a very simple example, after *Griffiths and Richards* [1989]: A given plate velocity, a constant exit point of the plume from the lower mantle and a simple shear flow in the upper mantle is assumed (top left). This gives rise to a parabolic conduit shape in the stationary case (top right). If the plate motion changes, the shape of the conduit will adjust to the new plate motion. During a time of adjustment, the hotspot surface position will move relative to the fixed source in a direction parallel to the difference of plate motion before and after the change (bottom left). Relative to the plate, this means that even if the plate motion changes discontinuously, the hotspot track does not have a sharp bend, but is curved with a radius of magnitude similar to the deflection of the conduit (bottom right).

to ambient mantle flow at that depth. Hence most of the time hotspot surface motion has a component representing flow at mid-mantle depth (that is, where the transition from "low" to "high" viscosity, hence from "fast" to "slow" conduit rising speed occurs). This flow is frequently toward ridges, opposite to plate motions and coherent under one plate. Secondly, if the conduit is already tilted below that depth and v_c is not negligible, another component of motion is due to conduit elements rising from different locations. Such a tilt is caused by shearing of the conduit due to variations of flow velocity with depth, and the corresponding component of hotspot motion represents the change of flow velocity with depth. Therefore, as a general tendency, with increasing age of a hotspot, its motion will represent flow at increasing depth: This is even exactly true in the simple case of an initially vertical conduit distorted in a time-independent horizontal flow field with no lateral variations: In this case, the surface motion at a time t after the conduit was vertical is equal to the flow speed at the depth from which the conduit element rose during time t, as can be easily shown.

In order to estimate the depth levels which thus may be represented in hotspot surface motion, we have to estimate v_c in the lower mantle: for a constant conduit radius r_c it should be approximately $v_c \sim 1/\eta_{out}$ (i.e. decrease by about a factor 100 in the model used here). If η_{in}/η_{out} is constant, it follows from eqns. 1 and 2 $v_c \sim 1/\sqrt{\eta_{out}}$ (i.e. decrease by about a factor 10 in the model used here). As we have shown, the increase of η_{in} with depth is likely less than the increase of η_{out}, hence v_c in most of the lower mantle will probably be less than 10 % of the upper mantle value, i.e. not more than a few mm/yr. For example, for $r_c = 100$ km (more than what would be expected from scaling of lab experiments, but less than tomographic images below Iceland would indicate) $\eta_{out} = 4 \cdot 10^{22}$ Pas and other values as before, we obtain $v_c \approx 1.3$ mm/yr. With a representative hotspot lifetime of $t_l = 100$ Ma, this indicates, that hotspot surface motion probably represents flow in the upper part of the lower mantle most of the time, and that flow in the lowermost mantle has little effect on hotspot motion.

v_c will not only decrease with depth in absolute terms, but also relative to ambient mantle flow speeds, as those do not decrease as strongly with depth: Numerical calculations of mantle convection with depth-dependent viscosity by *Gurnis* [1986] indicate that root mean square flow speeds decrease $\sim 1/\ln(\eta_{out})$ (i.e. by a factor of about 1/4.6 for a 100-fold viscosity increase), and our flow calculations give similar results, with typical flow speeds in the lower mantle of the order of 1 cm/yr. Therefore conduit motion in the lower mantle should be dominated by advection; the source regions of the plumes should move with the horizontal flow at the top of D" – frequently toward large-scale upwellings in the lower mantle. The lines of thought presented in this section are also illustrated in Figure 5. The mantle flow field that hence causes hotspot motion and conduit distortion is discussed in section 6.

4. EXTINCTION OF PLUME CONDUITS

In another laboratory experiment, *Whitehead* [1982] showed that plume conduits break up into separate drops if they become sufficiently distorted ($\gtrsim 60°$ from vertical – see Figure 6). However this result was again obtained for a chemical plume. *Richards and Griffiths* [1989] find that in thermal plumes the instability is surpressed by thermal entrainment, and that a plume conduit may be deflected to almost horizontal orientation without any instability. These results are for $r_c = 25$km and $\eta_{out} = 10^{21}$ Pa s when scaled to the mantle, therefore they are probably relevant at least for smaller plumes. A strongly tilted conduit may however be wiped out due to thermal entrainment effects (also demonstrated by *Richards and Griffiths*, [1989]) even without an instability developing.

An instability may not develop either during the lifetime t_l, if the viscosity of the surrounding mantle is sufficiently high. A simple estimate for that condition is that buoyant rising of one conduit diameter takes longer than t_l, i.e.

$$2r_c/v_c > t_l \tag{3}$$

With the above estimates we find that this may well be the case in (at least the lower part of) the lower mantle.

Finally, even if an instability develops and a conduit breaks up into drops in the uppermost mantle, the conduit beneath may remain intact if the drops rise fast enough such that enough material and heat is carried through the conduit to prevent extinction. We used a simple scaling argument to estimate

$$v_c \gtrsim 2l\kappa/r_c^2, \tag{4}$$

[*Steinberger and O'Connell,* 1998] where l is conduit length and κ is thermal diffusivity, which has been found to be of the order of $10^{-6}\mathrm{m}^2\mathrm{s}^{-1}$ for mantle materials [e.g., *Osako and Ito,* 1991].

In summary, a strong tilt therefore favors destruction of plume conduits. However extinction may also occur without a strong tilt, due to thermal entrainment, lack of material supply, etc. On the other hand conduits may survive despite a strong tilt.

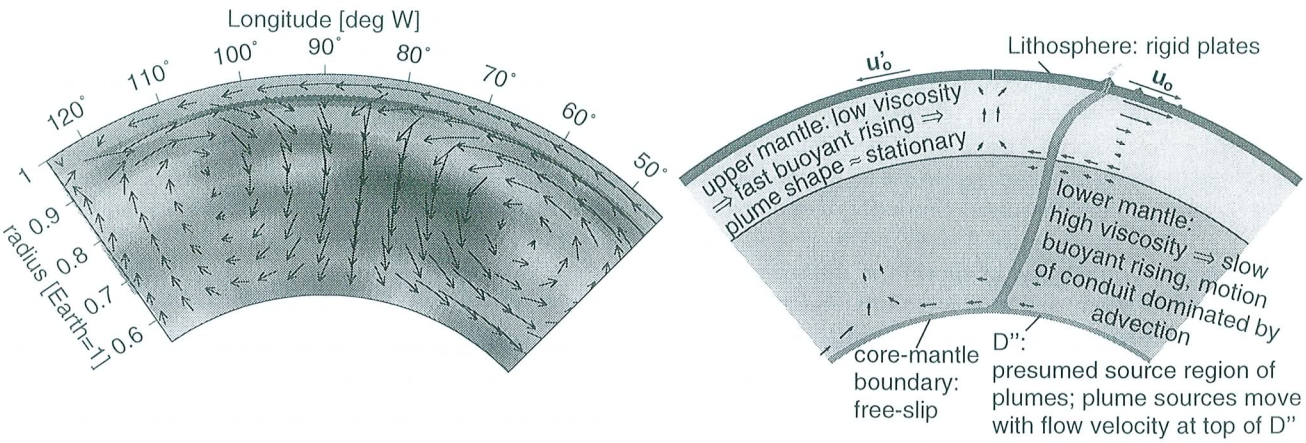

Figure 5. Left: Density anomalies beneath North America (model 3, i.e. inferred from Grand's tomographic model); cross section at 44.6 deg N; spherical harmonic expansion up to degree and order 32. Dark colors represent positive density anomalies (corresponding to fast anomalies in Grand's model), light colors represent negative anomalies (normalized to the maximum anomaly occurring in that depth layer). Also shown are arrows representing the E-W and vertical components of the induced present–day flow as calculated with the method of *Hager and O'Connell* [1979,1981] for viscosity model A. Length of arrows corresponds to displacement that would result from 50 Ma of constant flow. Right: Sketch showing how mantle flow may cause motion of hotspots and plume sources.

5. HOTSPOT MOTION VERSUS FIXITY – EVIDENCE FROM HOTSPOT TRACKS, PLATE RECONSTRUCTIONS AND PALEOMAGNETISM

The concept of hotspot fixity was first introduced after it was shown "that the Hawaiian-Emperor, Tuamotu-Line and Austral-Gilbert-Marshall island chains can be generated by the motion of a rigid Pacific plate rotating over three fixed hotspots" [*Morgan,* 1971]. More recent sampling shows that the age progression along the Tuamotu-Line and Austral-Gilbert-Marshall island chains is substantially more complicated than that expected from a single hotspot [*Jarrard and Clague,* 1977; *Duncan and Clague,* 1985; *Pringle and Duncan,* 1995; *McNutt et al.,* 1997]. Figure 7 however shows that geometry and age progression of several other hotspot tracks, in particular Hawaiian–Emperor and Louisville, can still be explained well by the fixed hotspot hypothesis. Of course, this is not a proof for hotspot fixity, since obviously hotspots moving coherently (i.e. without changing their distances) can explain the data equally well.

On the African hemisphere, the geometry and age progression of most hotspot tracks is not nearly as clear as for Hawaii and Louisville. *Müller et al.* [1993] showed that the fixed hotspot hypothesis is also compatible with the tracks there.

When looking at African and Pacific hotspot tracks combined, it becomes less clear whether hotspot fixity is in accord with observations. *Cande et al.* [1995] show a significant difference between the predicted Hawaiian hotspot track, assuming fixity relative to African hotspots, and the observed Hawaiian-Emperor chain. Their result is reproduced in Figure 8. The relative motion of Pacific and African hotspots, especially with regard to plate reconstructions in the Pacific-Antarctic region is also the subject of a paper by *Raymond et al.* [1999] in this volume. Another interpretation by *Harada* [1997] suggests that the Pacific and African hotspots are fixed within the uncertainties.

Another method to determine hotspot motion uses paleolatitude data that are inferred from the inclination of the characteristic remanent magnetization of drilled

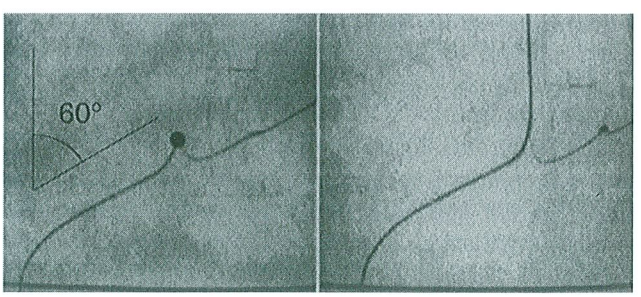

Figure 6. Laboratory experiment showing the breakup of a "chemical" plume conduit due to tilting. Figure after *Whitehead* [1982].

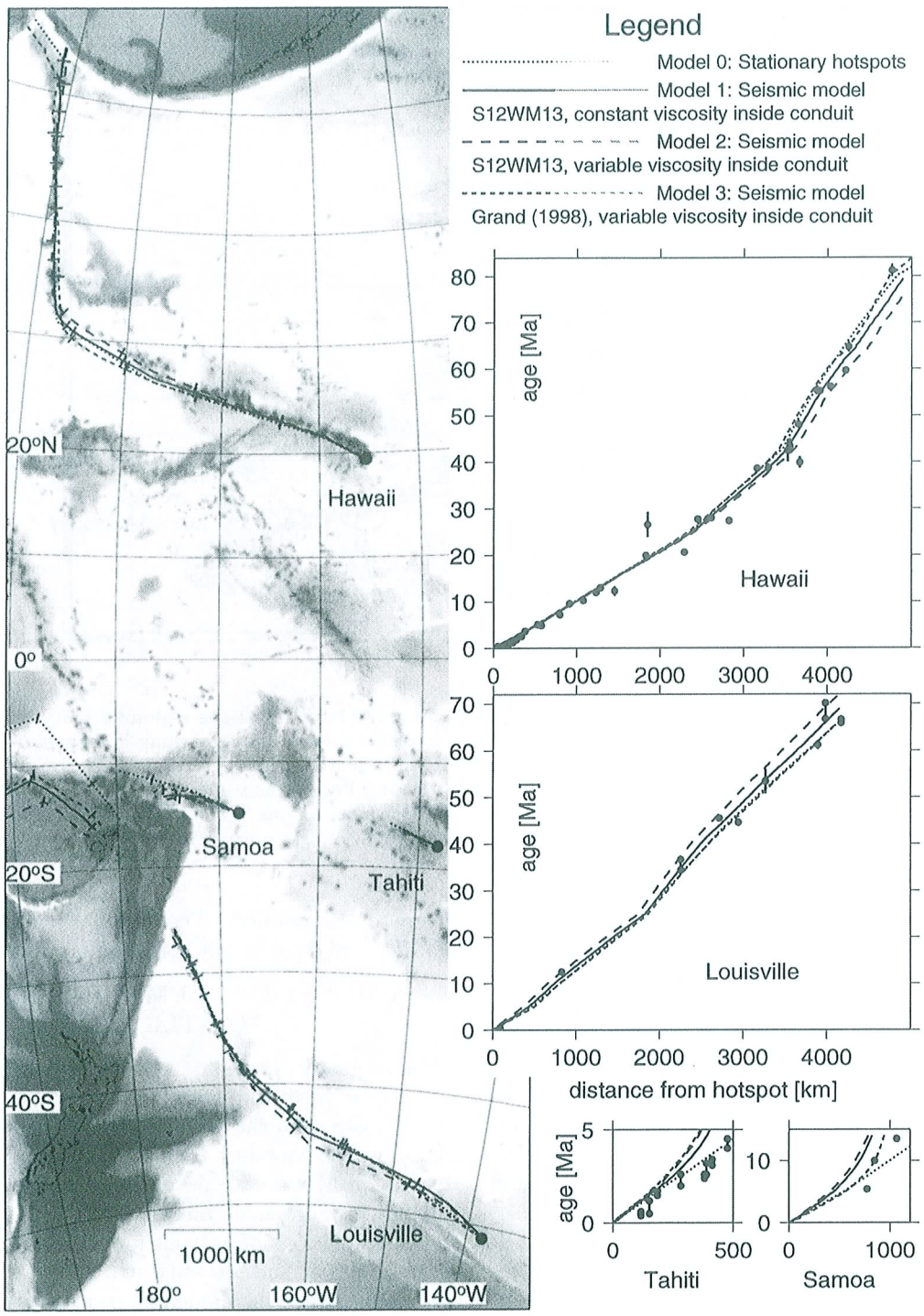

Figure 7. Hotspot tracks on the Pacific plate – observed and calculated for fixed and moving plumes (viscosity model A; three cases). Age data (shown as dots) for Hawaiian hotspot compiled by *Clague and Dalrymple* [1989] and from *Tarduno and Cottrell* [1997], for Louisville hotspot from *Watts et al.* [1988], for Tahiti and Samoa compiled by *Duncan and Clague* [1985]. Topography is shown in greyshades between -5000 and -2000 m, in uniform grey above -2000 m, and in white below -5000 m. Results for model B are also very similar.

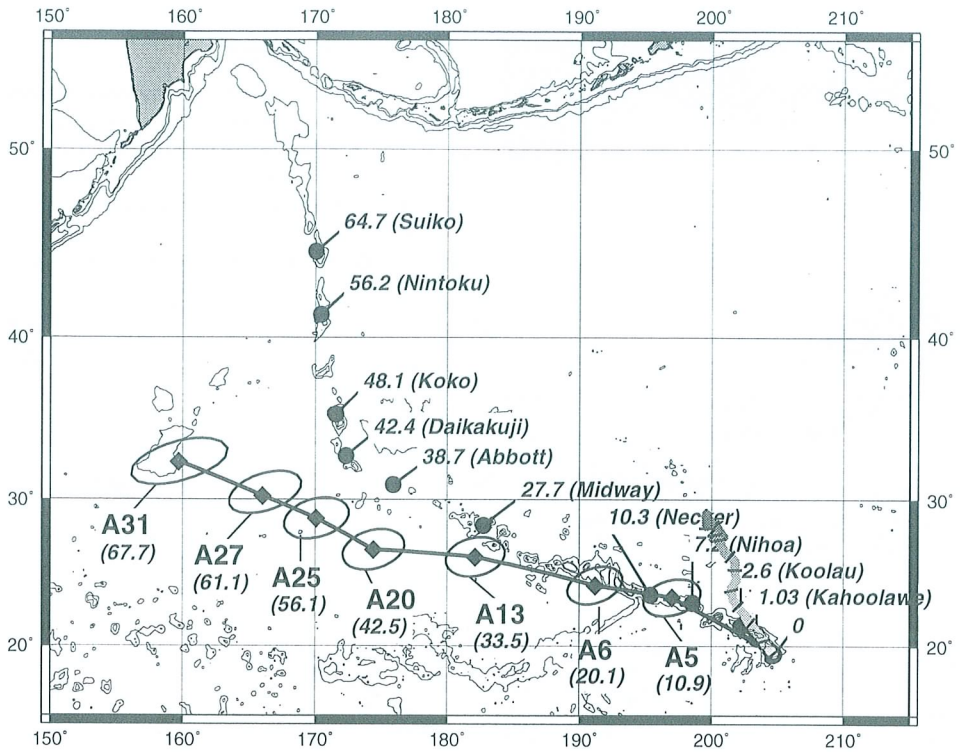

Figure 8. Prediction of the Hawaiian hotspot track from plate reconstructions assuming fixity relative to Indo-Atlantic hotspots. This prediction is different from the dotted line (assuming hotspot fixity) in Figure 7, because it is calculated for a given African absolute plate motion and a given relative motion Pacific vs. Africa, whereas in Figure 7 we use the best–fitting Pacific plate motion. Also shown is the motion of the Hawaiian hotspot (in the mean mantle reference frame of our flow calculations) as predicted from our model B, with greytones corresponding to age and tickmark interval 10 Ma. Figure modified after *Cande et al.* [1995].

basalts and sediment cores, using the axial dipole hypothesis: If all hotspots and the rotation axis were fixed relative to each other, the paleolatitude of hotspots should be the same as the present latitude for all times. This method can be extended to data other than from hotspot tracks: For a given model of absolute plate motion, based on hotspot tracks, the paleolatitude of any point on the plate can be predicted for all times, and compared with the observed paleolatitude. Using this method, *Sager and Bleil* [1987] find a "latitudinal shift of Pacific hotspots during the late Cretaceous and early Tertiary". In the top left panel of Figure 9 we redo their analysis, using our own model for the best fitting plate motion assuming fixed hotspots, and essentially reproduce their finding. Their results are however largely based on sediment cores and seamount paleomagnetism, which are less reliable than basalt cores. *Tarduno and Cottrell* [1997] have used data from basalt cores and find similar results, giving "evidence for motion of the Hawaiian hotspot during formation of the Emperor seamounts". The drawback here is that inclination data from basalt cores are far fewer in number.

6. A MODEL OF PLUMES IN LARGE–SCALE MANTLE FLOW

Since geodynamic models indicate that hotspots are unlikely to be fixed relative to one another, (as outlined in section 3) and the observational evidence for hotspot fixity versus mobility remains inconclusive (as shown in section 5) we have developed a numerical model of plumes in large–scale mantle flow. This enables us to make predictions of hotspot motion for various models of mantle flow and viscosity structure.

The details of the modelling procedure have been described elsewhere [*Steinberger and O'Connell*, 1998], so here we give only a brief overview with emphasis on understanding the physical processes: In a first step, a large–scale mantle flow field is calculated with the method of *Hager and O'Connell* [1979, 1981]. Using a spherical harmonic expansion, this method solves the

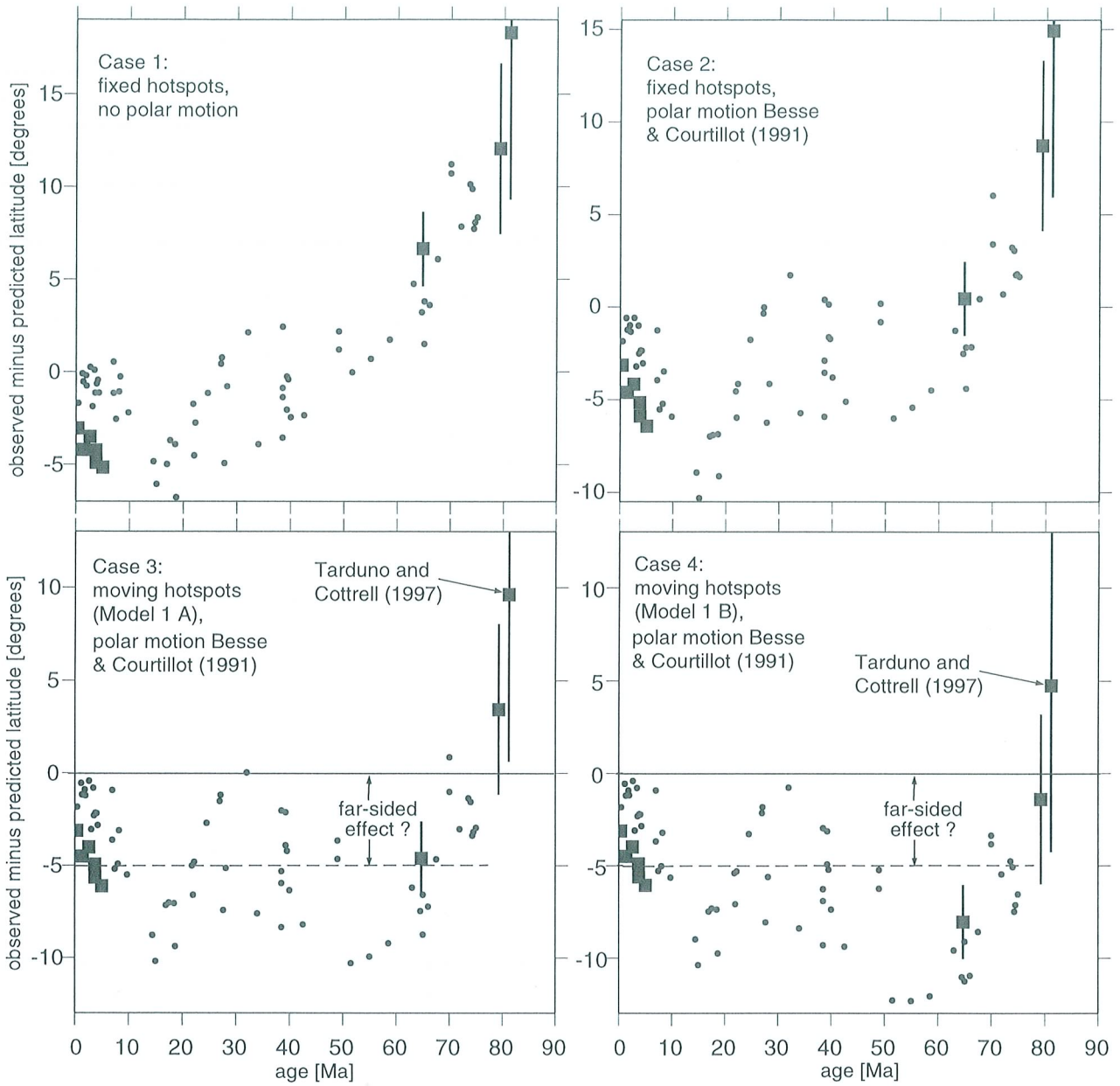

Figure 9. Latitudinal shift of Pacific hotspots – four cases. Observed paleolatitude data of samples on Pacific plate are from *Epp et al.* [1983], *Sager* [1984], *Sager and Bleil* [1987], *Tarduno and Gee* [1995], *Tarduno and Cottrell* [1997]. Larger squares represent more reliable data points (mostly on Hawaiian–Emperor chain). Similar to *Sager* [1984] we consider data points that are based on the paleomagnetism of extrusives, with a sufficiently large number of samples ($N \geq 18$), to be more reliable. For clarity, error bars (representing 95% confidence intervals) are only shown for more reliable data with ages ≥ 10 Ma. In the top left panel, predicted paleolatitudes are calculated by rotating samples from their drilling location back to the paleo-location where they were emplaced, using the measured age and a model of Pacific plate motion that optimizes the fit of the Hawaiian and Louisville hotspot tracks, assuming hotspot fixity. In the top right panel, the motion of the pole in the "fixed hotspot" reference frame is taken into account: In this case, the angular distance from the predicted paleo-location to the paleo-pole at the same age according to the *Besse and Courtillot* [1991] curve is the predicted paleo-latitude. In the two bottom panels, we use instead models of Pacific plate motion that optimize the fit of the Hawaiian and Louisville hotspot tracks, taking into account the calculated hotspot motion for two of our models (see Table 3).

equations of motion for a viscous mantle rheology, with viscosity varying with radius only. Because of the high viscosity, inertial forces are neglected.

Internal driving forces arise from mantle density heterogeneities $\delta\rho$ that are inferred from models of seismic s-wave speed anomaly δv_s. In most of the flow calculations shown here, we use either S12WM13 (by *Su et al.* [1994] – for our models 1 and 2), or the most recent model of S. Grand (retrieved via anonymous ftp and similar to *Grand et al.* [1997] – for our model 3). For viscosity model A, we use conversion factors $(\delta\rho/\rho) \,/\, (\delta v_s/v_s) = 0.2$ for S12WM13 resp. 0.4 for Grand's model, and only consider velocity heterogeneities below 220 km, in order to at least partly exclude effects of compositional continental roots. Both values are close to what has been inferred from geoid modelling [e.g., *Forte et al.,* 1993] and from laboratory experiments in combination with theoretical arguments [*Karato,* 1993]. A higher value is used for Grand's model because of the lower amplitudes of that model. For viscosity model B, we use conversion factors 0.4 for Grand's model and 0.2 for all other models at all depths, as in our previous paper, unless stated otherwise. The boundary conditions on the Earth's surface are taken to be the observed time–dependent global plate motions [*Gordon and Jurdy,* 1986; *Lithgow-Bertelloni and Richards,* 1998].

Mantle flow in our model is time-dependent for two reasons: First, plate motions change with time as the plate geometry changes and the velocities change; this changes the plate motion boundary condition that is applied to the model. Secondly, the flow field carries the internal density anomalies to new positions. We use the flow field to advect the density field backward in time from its present position for 68 Ma. This introduces some uncertainty in the model, since the advection is approximate. Nevertheless, the errors that accumulate over 68 My due to neglecting diffusion, viscous dissipation, adiabatic heating and cooling effects, are estimated to be relatively small. We have given a more detailed justification for the advection model in our previous work [*Steinberger and O'Connell,* 1998, appendix A2]. A constant density field is used before 68 Ma.

Figure 5 shows, as an example, a cross section below North America through model 3, as well as an inferred flow field. Note that both the density model and the calculated flow field are fully three–dimensional; we are however only able to plot the vertical and east-west component of the flow field. The dark structure in the center of the figure has been interpreted as the remains of the subducted Farallon plate, which are now in the lower mantle. As should be expected, this presumably cold and dense material drives a large–scale downward flow in our calculation. S12WM13 does not have as high resolution as more recent models such as Grand's. It does, however, provide a global model, which is needed to calculate a global flow field. In addition, the calculation of the flow provides an effective low–pass filter that averages the smaller scale features in the density field. Hence the lower resolution seismic models may still provide a sufficiently accurate flow field, especially in oceanic regions where more detailed tomographic results are not available. As an example, Figure 10 shows an inward flow at the base of the mantle towards an upwelling under southern Africa that corresponds to a large-scale negative seismic anomaly in this region. If Grand's model is used instead, the horizontal flow at the base of the mantle in this region is still dominated by this inward flow. Flow in the upper mantle is, to a larger degree, related to plate motions. Figures 10 and 11 show a flow at the top of the lower mantle that is frequently toward ridges i.e. has a "return flow" component opposite to plate motion. However, mantle flow in the depth range shown tends to be much slower than plate motions.

We then insert a plume conduit in the calculated large scale flow. We choose a vertical conduit as the initial condition, corresponding to the assumption that the plumehead that establishes the conduit (Figure 2) rises rapidly and is thus not significantly advected laterally. This assumption is discussed in more detail in *Steinberger* [1999]; here we just state that this assumption seems the most reasonable, because many hotspots are assumed rather old, such that the large-scale flow through which the plumehead has risen is poorly known, and also because an initially tilted conduit would further complicate the model by introducing more parameters. If a flood basalt is associated with the hotspot, we choose its age as the initial time. For example, for the Reunion hotspot we start with a vertical conduit 67 Ma ago (see Figure 1). All the ages used are listed in Table 1. The conduit is then advected and distorted in the flow field, whereby the velocity of each conduit element is a superposition of ambient mantle flow and vertical buoyant rising, as discussed in section 3.

Obviously, the separation of mantle flow in "plume flow" and "large scale flow" is somewhat artificial. For example, neither the flow into nor out of the conduit are considered. The separation is however justified since (a) plume conduits are expected to be thin features, as argued above, hence we expect their presence and

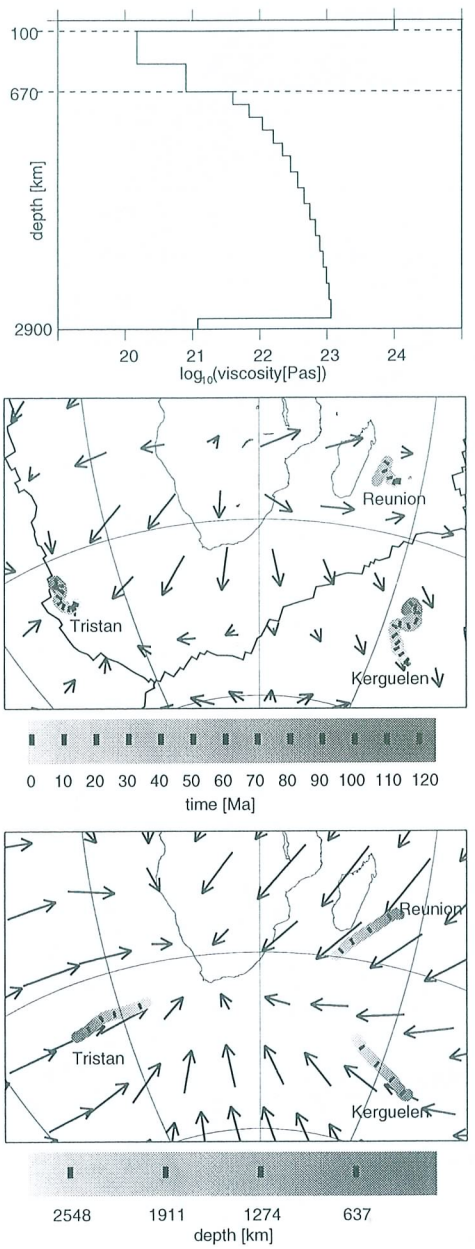

Figure 10. Calculated hotspot motion (mid-panel) and conduit shape (lower panel) for Tristan, Reunion and Kerguelen hotspots, for the viscosity model B shown. Arrows represent present–day flow at depths 800 km (mid-panel), resp. 2700 km (lower panel), with the arrow length corresponding to the total motion that would result from 68 Ma of constant flow. In the mid-panel, the motion of hotspots is plotted in the reference frame of the flow calculations (a mean mantle reference frame), with different shades of grey corresponding to different times, and tickmarks every 10 Ma. This hotspot motion is not to be confused with hotspot tracks on plates. In the lower panel, different shades of grey correspond to calculated conduit locations at different depths, with a tickmark interval of 0.1 Earth radii.

buoyancy does not significantly alter large-scale mantle flow, and (b) heat flow of plumes, hence their material flux is estimated to be substantially smaller than large-scale mantle flow: *Davies,* [1988] estimates that plumes supply less than 10 % of the total heat out of the mantle. Therefore we do not expect that inflow and outflow of plumes alters the large scale mantle flow field significantly either.

Based on eqns. (1) and (2), and in accordance with the discussion in section 3 we will use plume rising speeds as specified in Table 2, unless noted otherwise. Obviously these models are somewhat arbitrary. We therefore use several different models to show that results do not critically depend on exact values of v_c chosen (as was already argued in section 3 – see also *Steinberger* [1999] where results for more hotspots are shown).

Figure 10 is an example of our calculations, which illustrates what is described above: In the middle panel, the recent surface motion of the hotspots tends to be similar in direction and magnitude to the horizontal flow in the mid–mantle (here shown at depth 800 km). Whereas Tristan and Reunion show very little motion during the past 40 Ma, the motion of Kerguelen is quite significant, in a south–easterly direction. This coincides with *Morgan* [1981], who finds Kerguelen to be the least fixed hotspot in the Atlantic and Indian Oceans.

The lower panel shows the calculated shape of three conduits. The bases of the conduits are advected with the flow toward the large upwelling under South Africa. Since the flow in the mid and upper mantle is in quite different directions, there is a significant tilt of the conduits, with the base of the conduits closer to the upwelling under South Africa. Corresponding results for viscosity model A are shown in *Steinberger* [1999] and are very similar.

7. MOTION OF HOTSPOTS IN THE PACIFIC

Another example is shown in Figure 11. Here calculations are not for actual hotspots; instead the initial hotspot locations are on a ten degree grid. The motion of a hotspot is only shown if the conduit has not been tilted more than 60° at depths between 670 and 1070 km. The figure thus illustrates the regions where plumes, if present, could have survived and given rise to long–lived hotspots on the surface. We restrict ourselves to this depth range, as instabilities will develop slowly at greater depths, and will not necessarily lead to extinction at shallower depths, according to estimates 3 and 4. The "pattern" of surviving plumes calculated does not critically depend on this depth range chosen. Figure 11 can therefore help to explain the

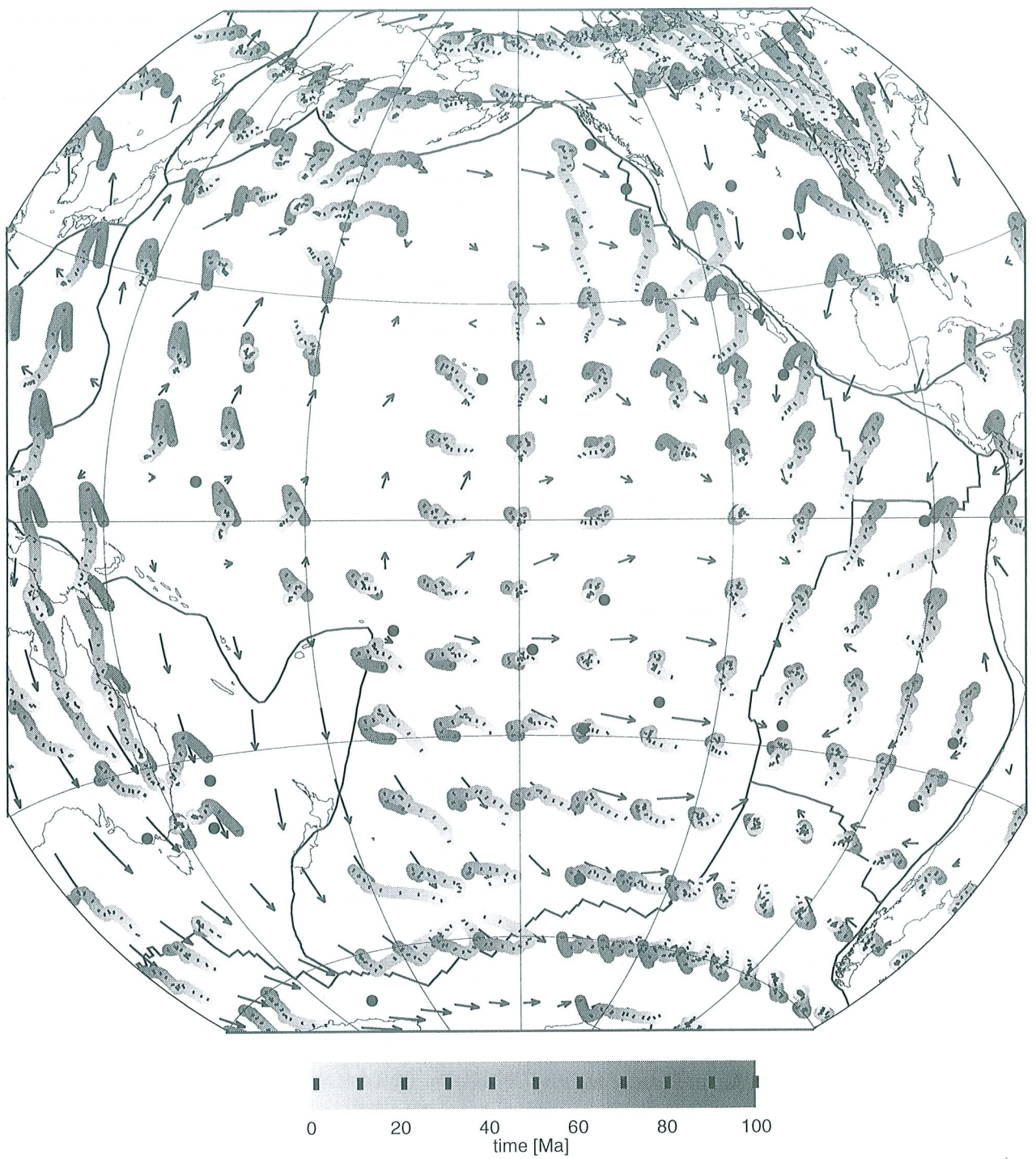

Figure 11. Motion and distribution of hypothetical hotspots (initially located on a 10-degree-grid) in the Pacific: Calculations are for model 1 A, with $v_c = 4$cm/yr for $\eta_{out} = 10^{21}$ Pas (i.e. 10 cm/yr below the lithosphere), corresponding to a conduit radius of 88 km according to eqn. 1. Motion is only plotted for plumes tilted $< 60°$ at depths between 670 and 1070 km. Initial surface positions of plumes are on a grid, with eruption of plumeheads 100 Ma ago. Arrows represent present–day flow at depth 1000 km, with the arrow length corresponding to the total motion in 50 Ma. Locations of actual hotspots are shown as black dots. Again, hotspot motion is plotted in the mean mantle reference frame.

observed hotspot distribution: In the regions of recent subduction and fast seismic anomalies, with the associated downward flow (see Figure 5), plume conduits frequently get tilted more than 60°, and the hotspots are more likely to become extinct. This agrees with the observation that hotspots cluster in the Pacific and around Africa, where tomography shows large–scale negative seismic anomalies in the lower mantle, hence large scale upwelling is inferred. The fact that Yellowstone is in a region of recent subduction is no contradiction to this, since its assumed age (equal to the Columbia River Basalts) is much less than 100 Ma: For this age (15 Ma) our models predict a Yellowstone conduit tilt of less than 60 degrees.

Results shown in Figure 11 are not specific for this particular viscosity structure – e.g. they are very similar for viscosity structure B [*Steinberger and O'Connell,* 1998, Figure 7]: both figures also show a coherent hotspot motion in a $\sim$ south-easterly direction over much of the Pacific plate, including the locations of Hawaii and Louisville. This motion corresponds to a largely coherent flow in the mid–mantle opposite to plate motion. During the first $\approx$ 10 Ma, hotspot motion tends to be in a different direction, as explained in section 3. For the actual parameters of the Hawaiian hotspot, the motion for model B is included in Figure 8. Results for actual hotspots are also shown in *Steinberger* [1999] for model A and in Figure 12 for a greater number of models: A coherent motion of Hawaii and Louisville remains a common feature of most models. As mentioned above, coherent hotspot motion yields tracks that are compatible with the assumption of hotspot fixity; therefore our result can help to reconcile the findings of *Morgan* [1971] and others with a convecting mantle. This is further illustrated in Figure 7: By choosing a different "best fitting" Pacific plate motion (Table 3), the calculated hotspot motions can fit the observed tracks and age progression about as well as assuming hotspot fixity. We note that especially for Tahiti the models with a moving hotspot do not fit the age progression as well as assuming hotspot fixity. This misfit occurs because in our model, during the first few Ma, the initially vertical conduit is being tilted towards a steady state, as explained above. There are no indications for such an effect in the observed age progression. This probably shows that, if volcanism in the Tahiti chain is due to a hotspot plume in the sense of the model discussed here, the tilt of its conduit did not significantly change during the past $\sim$ 5 Ma, in contrast to our model.

Table 2. Plume rising speeds (column 3) and corresponding variations (if any) of viscosity inside conduit (column 4) for a given model (column 1) and viscosity range outside conduit (column 2). $B_0 = 10^3$ kg/s and $\eta_0 = 10^{21}$ Pas are used; anomalous mass fluxes B are listed in Table 1. Model A requires larger values $v_c \cdot \eta_{out}$ than model B, because of the higher viscosity below the lithosphere. A higher ratio η_{in}/η_{out} is used in the layer of lowest viscosity in models 2 and 3 A, because that layer may be at least partly be fed by plumes [*Phipps Morgan et al.,* 1995], hence its viscosity may be closer to plume viscosity at the same depth.

Model	η_{out}	v_c [cm/yr]	η_{in}
1 A	all	$1.72 \cdot \sqrt{B/B_0} \cdot \eta_0/\eta_{out}$	const.
2/3 A	$\geq 10^{21}$ Pas	$1.36 \cdot \sqrt{B/B_0} \cdot \sqrt{\eta_0/\eta_{out}}$	$\sim \eta_{out}$
2/3 A	$\leq 10^{21}$ Pas	$1.36 \cdot \sqrt{B/B_0} \cdot \eta_0/\eta_{out}$	const.
B	all	$0.86 \cdot \sqrt{B/B_0} \cdot \eta_0/\eta_{out}$	const.

Below the Nazca plate the flow in the mid–mantle is in a very different direction than that under the Pacific, especially for model B [*Steinberger and O'Connell,* 1998, Figure 7]. We therefore expect a motion of the Easter hotspot relative to Hawaii and Louisville of up to several cm/year. Figure 13 shows that all models with hotspot motion, especially model B, fit the observed age progression better than the fixed hotspot model. Moreover, for model B the calculated hotspot motion yields a hotspot location that is, for the assumed plate boundary, actually on the Nazca plate for longer periods of time, thus further helping to explain the observed features (Nazca and Sala y Gomez ridges) that have been associated with the Easter hotspot. Predicted tracks considerably differ among each other, and none of them fits observations too well; detailed reconstructions of this track are difficult for several reasons: The present location of the Easter hotspot is uncertain; the speed of the Pacific plate between 0 and 25 Ma might be overestimated in our models (see Table 3); a hotspot location on the Pacific plate may also lead to features on the Nazca plate (and vice versa) owing to plume-ridge interaction; there have been ridge jumps that may lead to kinks in the ridge and segments with reversed age progression, but the past location of the ridge and the timing of the ridge jumps are poorly known. A more detailed investigation of this hotspot track might actually help to improve plate reconstructions in this region. For example, the ridge topography around $85°W$, $25°S$ might indicate such a kink. When interpreted that way, it would mean that the ridge jumped from east to west

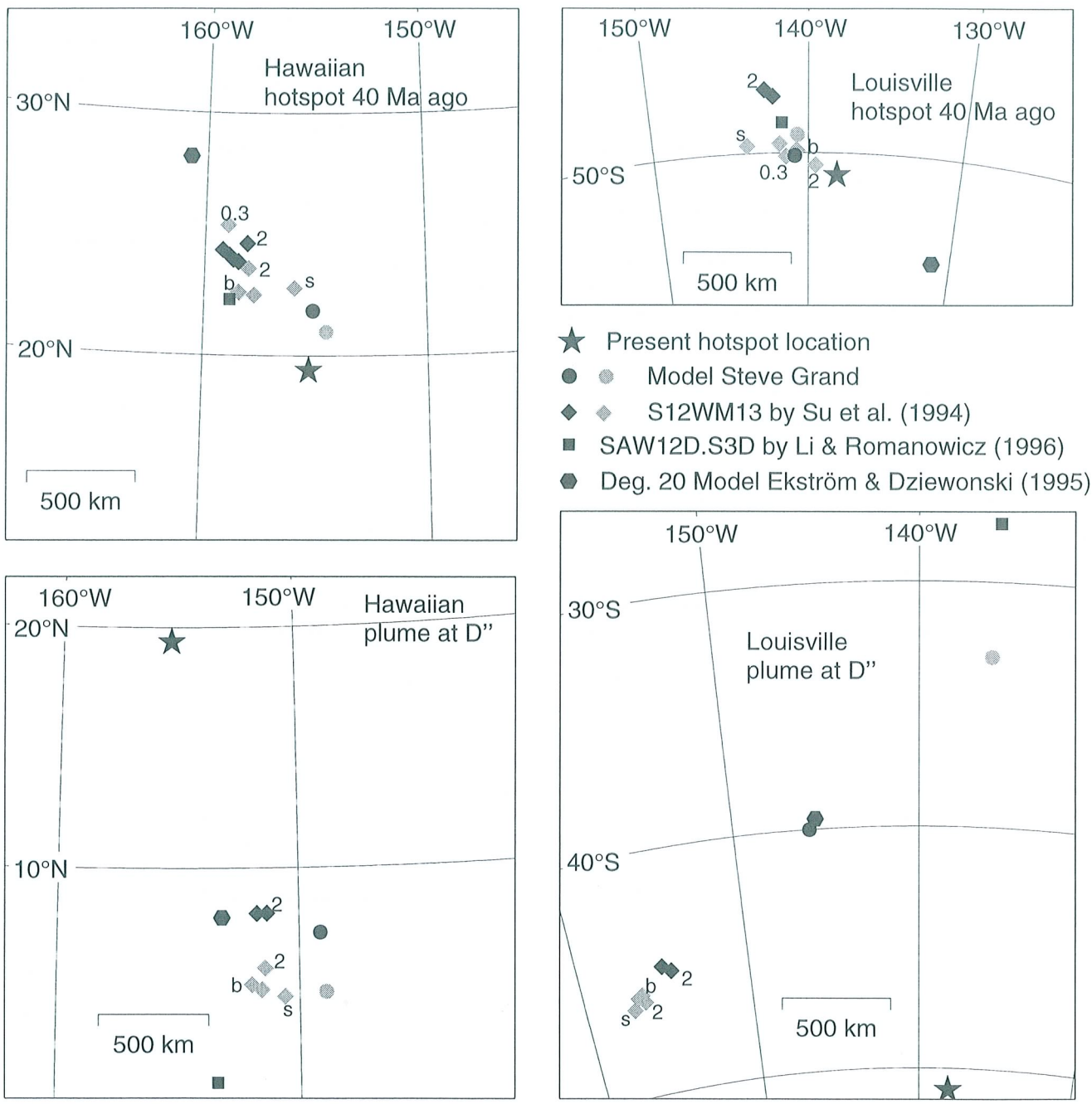

Figure 12. Summary of results for Hawaiian and Louisville hotspot for a greater number of models. Calculated hotspot surface locations 40 Ma ago (in mean mantle reference frame) and predicted locations of base of conduit at D" are shown. Results are shown for the viscosity models A (grey symbols) and B (black symbols). Grey symbols marked with a number "2" are for Model 2 (Table 2), whereas for black symbols marked with "2", $v_c = 0.86$ cm/yr $\cdot \sqrt{B/B_0} \cdot \sqrt{\eta_0/\eta_{out}}$ is used. For the data point marked with "0.3", a constant conversion factor $(\delta\rho/\rho)\,/\,(\delta v_s/v_s) = 0.3$ is used, otherwise conversion is done as specified in the text. The top left panel contains four black diamonds for assumed hotspot ages 100, 110, 120 and 130 Ma. Grey diamonds marked with the letter "b" (for big) and "s" (for small) correspond to buoyant rising speed increased resp. reduced by 50 %. Density anomalies are advected for 68 Ma in all cases except for black circles. Presumed present locations of Hawaiian and Louisville hotspots are shown as stars.

Table 3. Table of "absolute" Pacific plate rotations in a mean mantle reference frame. These were re-determined for the time intervals given in the first column (in Ma) for fixed hotspots (Model 0) and four models of moving hotspots. Our method of determining "best-fitting" plate motions is described in *Steinberger* [1999]. For each time interval, a constant rotation rate vector is assumed. Vectors are given in spherical coordinates (latitude[deg],longitude[deg],magnitude[deg/Ma]). Before 80 Ma, plate motions were not re-determined but adopted from *Lithgow-Bertelloni and Richards* [1998].

	Model 0			Model 1 A			Model 2 A			Model 3 A			Model B		
t [Ma]	lat	lon	mag	lat	lon	mag	lat	lon	mag	lat	lon	mag	lat	lon	mag
0– 5	-64	99	1.00	-64	101	0.94	-65	97	0.93	-65	90	1.03	-64	107	0.91
5–25	-73	122	0.87	-77	110	0.82	-77	97	0.84	-74	133	0.86	-79	92	0.80
25–43	-59	122	0.58	-55	156	0.51	-57	157	0.51	-63	151	0.57	-56	168	0.48
43–80	-8	105	0.59	1	104	0.55	1	101	0.56	-7	104	0.54	-7	99	0.49

of the hotspot around 22 Ma ago, and the hotspot has remained beneath the Nazca plate since then. The observed age progression (indicating a steeper slope in the age vs. distance plot $\approx$ 20 Ma ago) might even result from a change of plume tilt from toward the west (due to Pacific plate motion) to toward the east (due to Nazca plate motion), as discussed above. For comparison, in the plate boundary model used here, a ridge jump over the plume occurs 10 Ma ago, and the predicted age vs. distance curves have a steeper slope following that ridge jump. More age data would however be required to support such an interpretation.

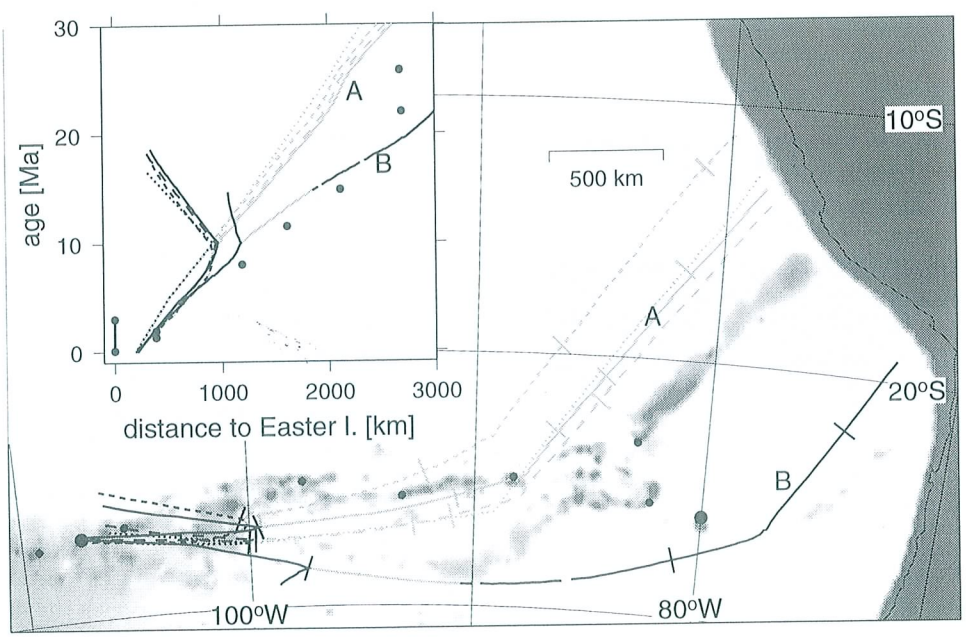

Figure 13. Easter hotspot track and age progression on the Nazca plate – Data [*O'Connor et al.*, 1995, and references herein] (shown as dots) and calculations for fixed and moving hotspots (four cases – legend see Figure 7); two solid lines are for viscosity models A and B as indicated. Assumed hotspot ages are 100 Ma for model A and 60 Ma for model B; if a significantly older age is assumed for model B, the calculated plume conduit is severely distorted. Location of the Easter hotspot is assumed half-way between Easter and Sala y Gomez Islands, as inferred from extrapolating age data on Sala y Gomez Ridge. Following previous suggestions [*O'Connor et al.*, 1995; *Morgan*, 1978], it is assumed that Easter Island is due to channeling of plume material toward the ridge. Black lines show the calculated hotspot track for the model of past plate motions and geometry used [*Gordon and Jurdy*, 1986]; segments with reversed age progression occur when the calculated hotspot location is on a part of the Pacific plate that subsequently gets transferred to the Nazca plate according to the model. Grey lines are calculated assuming the hotspot is always located on the Nazca plate regardless of any model of plate boundaries.

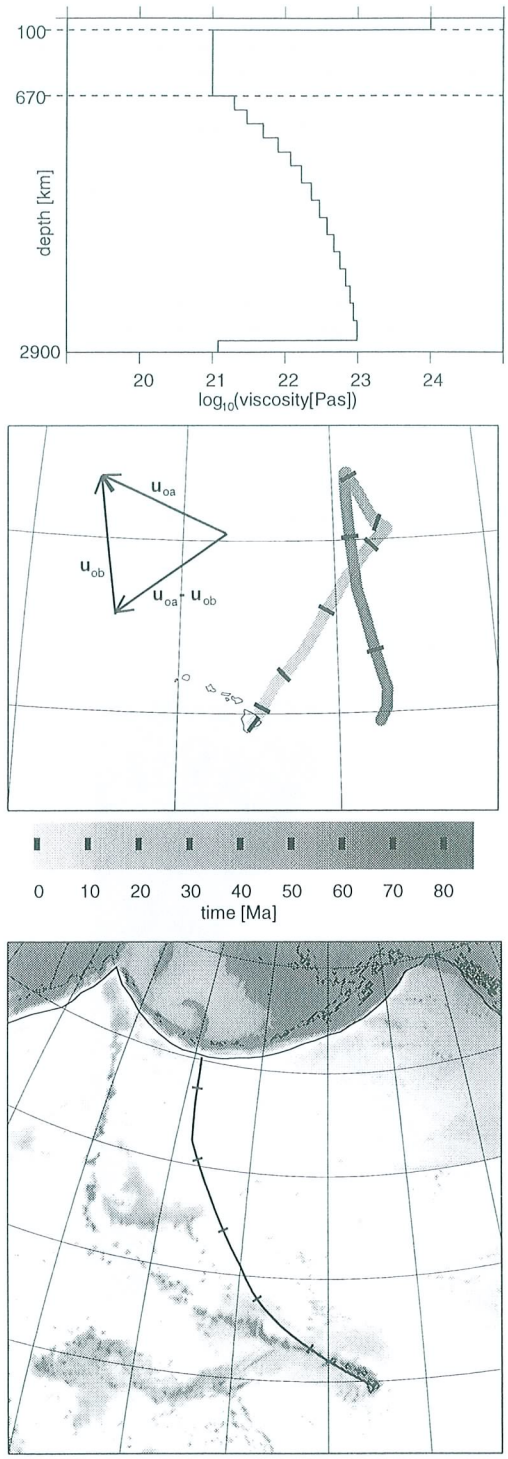

Figure 14. Calculated hotspot motion and track for Hawaiian plume, for viscosity model C (top panel). Predicted hotspot motion (in mean mantle reference frame) is shown in mid-panel, along with arrows indictating plate motions before and after 43 Ma, and the difference. The bottom panel shows the predicted hotspot track on the Pacific plate.

So far we have concentrated on model results that correspond well with observations. We conclude this section by showing a model that does not fit the observations, thus constraining the range of acceptable models. Figure 14 shows a result for a viscosity structure, similar to model B, but without the channel of low viscosity beneath the lithosphere, and with v_c as in Table 2 for model B. The bottom panel shows that this model cannot reproduce the observed sharp bend of the Hawaiian-Emperor chain; rather it exhibits a fairly wide arc. In this model (C) the buoyant rising speed of the plume in the uppermost viscosity layer below the lithosphere is much less, and hence the deflection x_0 much larger, than in the previous models A and B. As we already saw for the simple model in Figure 4, the mid-panel of Figure 14 shows the hotspot moving approximately parallel to $\mathbf{u}_{0a} - \mathbf{u}_{0b}$ during a time following the change in plate velocity from $\mathbf{u}_{0b}$ to $\mathbf{u}_{0a}$. According to Figure 4 and Table 2, we should expect a horizontal plume deflection $x_0 \approx 90 - 150$km in the uppermost viscosity layer for models A and B, whereas $x_0 \approx 1150$km for model C, and a similar radius of curvature of the bend. Both results roughly agree with the respective numerical results shown in Figures 7 and 14, but only the first one is compatible with the observed sharp bend.

The results for model C thus indicate that a layer of low viscosity underlying the lithosphere is necessary to explain the observed hotspot tracks. While details of the mantle viscosity structure may not be constrained by these models, we can also conclude that a relatively high viscosity in at least parts of the lower mantle is required, simply in order to keep the mantle flow speeds low enough to achieve relative hotspot motions in accordance with observations. Examples were shown in *Steinberger and O'Connell* [1998].

8. IMPLICATIONS OF HOTSPOT MOTION FOR PLATE TECTONICS

In Figure 8, the calculated motion of the Hawaiian hotspot is shown together with the discrepancy between the observed Hawaiian hotspot track and the prediction assuming fixity relative to Indo-Atlantic hotspots, according to *Cande et al.* [1995]. Back to 43 Ma, the time of the bend of the Hawaiian–Emperor chain, the calculated hotspot motion explains the difference between the observed track and the prediction of *Cande et al.* [1995]. Before that however, the calculated motion of the hotspot is not sufficient to explain the discrepancy. Figure 12 shows that – independent of which tomographic model, viscosity structure, etc. is chosen – many models can significantly reduce that difference

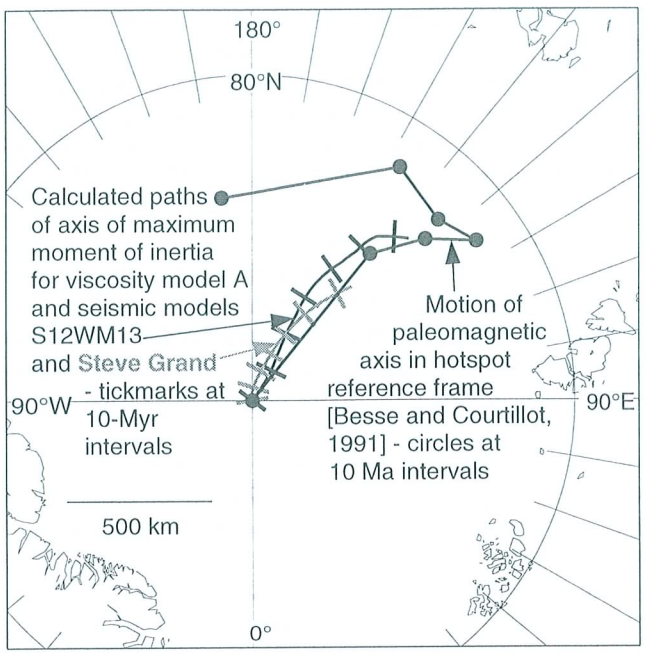

Figure 15. True polar wander – comparison of a curve based on paleomagnetic results with model calculations of changes of the principal axis of inertia due to advection of mantle density heterogeneities. The latter are inferred from the tomographic models S12WM13 [*Su et al.*, 1994] and from Grand's latest model (as in models 1/2 and 3), for viscosity model A, otherwise the model is the same as in *Steinberger and O'Connell* [1997]. Results for viscosity model B are considerably different; more generally, only viscosity models that are compatible with geoid modelling tend to yield true polar wander curves in agreement with paleomagnetic evidence.

during the last 43 Ma. None of the models, though, even approximately explains the much larger misfit before 43 Ma.

In Figure 9, the observed minus predicted latitudes on the Pacific plate are plotted under four different assumptions. As mentioned above, in the first case, which takes into account neither polar motion nor hotspot motion, a significant shift with time occurs. This shift is greatly reduced if polar motion, according to the curve of *Besse and Courtillot* [1991] is taken into account. That curve is inferred from continental paleomagnetic data, and is therefore independent of data from the Pacific plate. While details remain uncertain, a polar motion of 5 to 10 degrees from $\sim$ 160° E toward the present pole during the past $\sim$ 50 Ma is a common feature of several models of true polar wander [e.g., *Andrews,* 1985; *Livermore et al.,* 1984]. It is also supported by numerical models of polar motion based on calculated changes of the degree two geoid caused by advection of mantle density heterogeneities which we performed [*Steinberger and O'Connell,* 1997]. Figure 15 shows results for viscosity model A and the two tomographic models mainly used here: directions and magnitudes during the past $\approx$ 50 Ma are similar to the models based on paleomagnetism. Similar calculations, based on subduction history, were also recently performed by *Richards et al.* [1997].

In the lower panels of Figure 9, hotspot motion is also taken into account, and the best-fitting Pacific plate motion is re–determined. Because of the largely coherent hotspot motion opposite to plate motion, these models yield slower plate motions with a smaller northward component than the model with fixed hotspots. Additionally, the motion of the African plate is re–determined based on the calculated motion of the Reunion and Tristan hotspots shown in Figure 10. By considering the difference between our re–calculated motion of the African plate and its motion in the hotspot reference frame that was used by *Besse and Courtillot* [1991], their curve is converted into the same mean-mantle reference frame in which our calculations are done. The effects of this step are small (especially between 0 and 40 Ma) however, because of the small hotspot motion calculated during that time.

When these effects are included, there is essentially no trend in observed minus predicted paleolatitudes between 0 and 70-80 Ma. Figure 12 shows that the amounts of hotspot motion in the two models included in Figure 9 are fairly typical for a larger number of models, which will therefore all approximately remove any trend during that period. However there is a significant systematic offset from zero. The horizontal line through the data points is drawn by hand. An offset is even apparent in data from lava flows on the Hawaiian Island of ages 0 to 5 Ma. These data points are averaged over a large number of samples such that short term secular variations should be averaged out, and are considered more reliable [*Sager,* 1984]. It would be difficult to explain this offset of several degrees during the past 5 Ma by a hotspot motion unaccounted for in our model, especially since the Hawaiian track during the past 5 Ma gives no indication for a significant hotspot motion. The offset is therefore very likely due to other reasons and we conclude that the removal of any trend indicates that our models describe hotspot motion adequately, at least back to $\sim 70 - 80$ Ma ago.

The data point for Detroit Seamount (81 Ma) by *Tarduno and Cottrell* [1997] however is offset significantly from all other points. To determine whether this is due to hotspot motion more rapid than in our model, an episode of rapid true polar wander not accounted for

in the *Besse and Courtillot* [1991] curve, or long-lived non-dipolar components in the Earth's magnetic field will clearly require more data. The offset in paleolatitude in Figure 9 may reflect a feature of the field that is persistent over relatively long times [*Johnson and Constable,* 1998].

9. DISCUSSION AND OUTLOOK

The purpose of this paper was to discuss the problem of hotspot motion from a geodynamic viewpoint. This problem is motivated by observations – some of them support the idea of hotspot fixity, others seem to require significant motions of hotspots. Following a general introduction to the current ideas about plumes and hotspots, we therefore reviewed these observations. We then presented a numerical model that is intended to explain most of the observations. In this context, the introduction also served to justify why this particular numerical approach was taken. Numerical results are shown here for only a few representative hotspots, where effects can be seen well, and/or results have important implications regarding plate motions. A more systematic treatment of all known hotspots is given in *Steinberger* [1999].

A coherent motion of Hawaiian and Louisville hotspots of the order of 1 cm/yr and a southward component of Hawaiian hotspot motion of similar magnitude during the Cenocoic is feature of most models tested. Our results therefore explain the apparent misfit between observed and predicted Hawaiian hotspot track that has been reported by *Cande et al.* [1995] only back to 43 Ma. Where the remaining misfit comes from and to what extent unrecognized plate boundaries can change the results is the subject of ongoing research [*Raymond et al.*, this issue]. In combination with polar wander, paleomagnetic data can however be explained back to about 70-80 Ma. This result does not depend on the particular polar wander curve chosen, as a polar motion of the order of 5 degrees away from the Pacific during the Cenocoic is a common feature of several paleomagnetic true polar wander curves as well as our predictions from the advection of mantle density heterogeneities. 5 degrees from polar motion plus about 7 to 8 degrees from hotspot motion are sufficient to explain the previously reported trend in observed minus predicted paleomagnetic data back to about 70-80 Ma. Our results do not support the hypothesis of a particularly rapid motion of the Hawaiian hotspot before 43 Ma, as proposed by *Norton* [1995], therefore a rather abrupt change in absolute plate motion at around 43 Ma for the Pacific plate is required, accompanied by corresponding adjustments in the motions of surrounding plates. Our results also give predictions of the shape of plume conduits: Plume source locations tend to be displaced relative to corresponding surface hotspots, approximately towards the center of large-scale upwellings under Southern Africa and the South Pacific (Figures 10 and 12).

We have shown that not all models for "reasonable" parameters (i.e. in agreement with other evidence) give results in agreement with observations. Therefore, our models can help to further constrain model parameters such as viscosity structure. Comparison of various models introduced here and in our other papers, that are in agreement with observations, shows that we can make reasonably robust predictions of direction and magnitude of hotspot motion and of the tilt of plume conduits. In general, predictions do not depend on particular model parameters chosen, but are similar for a great number of models. Because of model uncertainties, obviously no detailed predictions can be made at present. The validity of our predictions and hence of the proposed underlying physical mechanism is supported by the fact that our model can help to explain a number of previously unexplained observations, particularly for more recent times. The examples shown here focussed on the Hawaiian, Louisville and Easter hotspots and hence plate motions in the Pacific region. In other instances, significant misfits remain. We anticipate that, due to better model constraints, we will be able to make more accurate predictions of hotspot motion in the future, and that, in combination with better constraints on plate reconstructions and a greater number of paleomagnetic data, remaining misfits can be resolved.

Acknowledgments. We thank Steve Grand for sharing his latest, unpublished model via anonymous ftp. Some of the calculations were done by Maria Antretter. Based on comments by Carol Raymond, Mark Richards and an anonymous reviewer, the initial manuscript was profoundly rewritten. Consistency of viscosity structure A with models of the geoid was checked using a code written by Svetlana Panasyuk.

REFERENCES

Albers, M., and U. R. Christensen, The excess temperature of plumes rising from the core-mantle boundary, *Geophys. Res. Lett., 23*, 3567-3570, 1996.

Andrews, J. A., True polar wander: An analysis of cenozoic and mesozoic paleomagnetic poles, *J. Geophys. Res., 90*, 7737-7750, 1985.

Besse, J., and V. Courtillot, Revised and synthetic apparent polar wander paths of the African, Eurasian, North American and Indian plates, and true polar wander since 200 Ma, *J. Geophys. Res., 96*, 4029-4050, 1991.

Bijwaard, H., and W. Spakman, Tomographic evidence for a

narrow whole mantle plume below Iceland, *Earth Planet. Sci. Lett., 166*, 121-126, 1999.

Cande, S. C., C. A. Raymond, J. Stock, and W. F. Haxby, Geophysics of the Pitman Fracture Zone and Pacific-Antarctic plate motions during the Cenozoic, *Science, 270*, 947-953, 1995.

Chopelas, A., and R. Boehler, Thermal expansion measurements at very high pressure, systematics, and a case for a chemically homogeneous mantle, *Geophys. Res. Lett., 16*, 1347-1350, 1989.

Choubert, G., and A. Faure-Muret, Atlas geologique du monde, *Commission de la carte geologique du monde*, Unesco, Paris, 1976.

Clague, D. A., and G. B. Dalrymple, Tectonics, geochronology, and origin of the Hawaiian-Emperor volcanic chain, in *The Geology of North America*, Vol. N, *The Eastern Pacific Ocean and Hawaii*, edited by E. L. Winterer, D. M. Hussong, and R. W. Decker, pp. 188-217, GSA, Boulder, CO., 1989.

Davies, G. F., Ocean bathymetry and mantle convection, 1. Large-scale flow and hotspots, *J. Geophys. Res., 93*, 10467-10480, 1988.

Davies, G. F., Temporal variation of the Hawaiian plume flux, *Earth Planet. Sci. Lett., 113*, 277-286, 1992.

Duncan, R. A., and D. A. Clague, Pacific plate motion recorded by linear volcanic chains, in *The Ocean Basins and Margins*, vol. 7a, edited by A. E. M. Nairn, F. G. Stehli, and S. Uyeda, pp. 89-121, Plenum, New York, 1985.

Duncan, R. A., and R. B. Hargraves, $^{40}Ar/^{39}Ar$ geochronology of basement rocks from the Mascarene Plateau, the Chagos Bank, and the Maldive Ridge, *Proc. Ocean Drill. Program Sci. Results, 115*, 43-51, 1990.

Ekström, G., and A. M. Dziewonski, Improved models of upper mantle S velocity structure (abstract), *Eos Trans. AGU, 76, Fall Meet. Suppl.*, F421, 1995.

Epp, D., W. W. Sager, F. Theyer, and S. R. Hammond, Hotspot-spin axis motion or magnetic far-sided effect? *Nature, 303*, 318-320, 1983.

Forte, A. M., A. M. Dziewonski, and R. L. Woodward, Aspherical structure of the mantle, tectonic plate motions, nonhydrostatic geoid, and topography of the core-mantle boundary, in *Dynamics of the Earth's Deep Interior and Earth Rotation, Geophys. Mon. Ser.*, Vol. 72, edited by J.-L. Le Mouël, D. E. Smylie, and T. Herring, pp. 135-166, AGU, Washington, DC., 1993.

Gordon, R. G., and D. Jurdy, Cenocoic global plate motions, *J. Geophys. Res., 91*, 12389-12406, 1986.

Grand, S. P., R. D. Van der Hilst, and S. Widiyantoro, Global seismic tomography: A snapshot of convection in the Earth, *GSA Today, 7*, 1-7, 1997.

Griffiths, R. W., and I. H. Campbell, Stirring and structure in mantle plumes, *Earth Planet. Sci. Lett., 99*, 66-78, 1990.

Griffiths, R. W., and M. A. Richards, The adjustment of mantle plumes to changes in plate motion, *Geophys. Res. Lett., 16*, 437-440, 1989.

Gurnis, M., Convective mixing in the Earth's mantle, Ph. D. Thesis, Aust. Nat. Univ., Canberra, 1986.

Hager, B. H., and R. J. O'Connell, Kinematic models of large-scale flow in the Earth's mantle, *J. Geophys. Res., 84*, 1031-1048, 1979.

Hager, B. H., and R. J. O'Connell, A simple global model of plate dynamics and mantle convection, *J. Geophys. Res., 86*, 4843-4867, 1981.

Harada, Y., New accurate models of the plate motions relative to the hotspots and the cause of the discrepancy in the global plate-motion circuit (abstract), *Eos Trans. AGU, 78, Fall Meet. Suppl.*, F721, 1997.

Haskell, N. A., The motion of a fluid under a surface load, 1, *Physics, 6*, 265-269, 1935.

Jarrard, R. D., and D. A. Clague, Implications of Pacific island and seamount ages for the origin of volcanic chains, *Rev. Geophys. Space Phys., 15*, 57-76, 1977.

Johnson, C. L., and C. G. Constable, Persistently anomalous Pacific geomagnetic fields, *Geophys. Res. Lett., 25*, 1011-1014, 1998.

Karato, S., Importance of anelasticity in the interpretation of seismic tomography, *Geophys. Res. Lett., 20*, 1623-1626, 1993.

Lambeck, K., and P. Johnston, The viscosity of the mantle: evidence from analyses of glacial-rebound phenomena, in *The Earth's Mantle*, edited by I. Jackson, pp. 461-502, Cambridge University Press, Cambridge, 1998.

Li, X.-D. and B. Romanowicz, Global mantle shear velocity model developed using nonlinear asymptotic coupling theory, *J. Geophys. Res., 101*, 22245-22272, 1996.

Lithgow-Bertelloni, C., and M. A. Richards, The dynamics of Cenozoic and Mesozoic plate motions, *Rev. Geophys., 36*, 27-78, 1998.

Livermore, R. A., F. J. Vine, and A. G. Smith, Plate motions and the geomagnetic field - II. Jurassic to Tertiary, *Geophys. J. R. astr. Soc., 79*, 939-961, 1984.

Manga, M., H. A. Stone, and R. J. O'Connell, The interaction of plume heads with compositional discontinuities in the Earth's mantle, *J. Geophys. Res., 98*, 19979-19990, 1993.

McNutt, M. K., D. W. Caress, J. Reynolds, K. A. Jordahl, and R. A. Duncan, Failure of plume theory to explain midplate volcanism in the southern Austral islands, *Nature, 389*, 479-482, 1997.

Mitrovica, J. X., Haskell [1935] revisited, *J. Geophys. Res., 101*, 555–569, 1996.

Mitrovica, J. X., and A. M. Forte, Radial profile of mantle viscosity: Results from the joint inversion of convection and postglacial rebound observables, *J. Geophys. Res., 102*, 2751–2769, 1997.

Morgan, W. J., Convection plumes in the lower mantle, *Nature, 230*, 42-43, 1971.

Morgan, W. J., Deep mantle convection plumes and plate motions, *Am. Assoc. Pet. Geol. Bull., 56*, 203-213, 1972.

Morgan, W. J., Rodriguez, Darwin, Amsterdam,.., a second type of hotspot island, *J. Geophys. Res., 83*, 5355-5360, 1978.

Morgan, W. J., Hotspot tracks and the opening of the Atlantic and Indian Oceans, in *The Sea*, Vol. 7, *The oceanic lithosphere*, edited by C. Emiliani, pp. 443-487, Wiley, New York, 1981.

Müller, R. D., J.-Y. Royer, and L. A. Lawver, Revised plate motions relative to the hotspots from combined Atlantic and Indian Ocean hotspot tracks, *Geology, 21*, 275-278, 1993.

National Geophys. Data Center, ETOPO-5 bathymetry/topography data, *Data Announc. 88-MGG-02*, Natl. Oceanic

& Atmos. Admin., U.S. Dep. Commer., Boulder, Colo., 1988.

Norton, I. O., Plate motions in the North Pacific: The 43 Ma nonevent, *Tectonics, 14*, 1080-1094, 1995.

O'Connor, J. M., P. Stoffers, and M. O. McWilliams, Time-space mapping of Easter Chain volcanism, *Earth Planet. Sci. Lett., 136*, 197-212, 1995.

Olson, P., and H. Singer, Creeping plumes, *J. Fluid Mech., 158*, 511-531, 1985.

Osako, M., and E. Ito, Thermal diffusivity of $MgSiO_3$ perovskite, *Geophys. Res. Lett., 18*, 239-242, 1991.

Phipps Morgan, J., W. J. Morgan, Y.-S. Zhang, and W. H. F. Smith, Observational hints for a plume–fed, suboceanic asthenosphere and its role in mantle convection, *J. Geophys. Res., 100*, 12753-12767, 1995.

Pringle, M. S., and R. A. Duncan, Radiometric ages of basement lavas recovered at Loen, Wodejebato, MIT and Takuyo-Daisan Guyots, northwestern Pacific Ocean, *Proc. Ocean Drill. Program Sci. Results, 144*, 547-560, 1995.

Raymond, C. A., J. M. Stock, and S. C. Cande, Fast Paleogene motion of the Pacific hotspots from revised global plate circuit constraints, in *The History and Dynamics of Global Plate Motions*, Geophys. Mon. Ser., edited by M. A. Richards, R. G. Gordon, and R. D. van der Hilst, AGU, Washington, DC., 1999.

Ricard, Y., L. Fleitout, and C. Froidevaux, Geoid heights and lithospheric stresses for a dynamic Earth, *Ann. Geophys., 2*, 267-286, 1984.

Richards, M. A., Hotspots and the case for a high viscosity lower mantle, in *Glacial Isostasy, Sea-Level and Mantle Rheology*, edited by R. Sabadini, K. Lambeck, and E. Boschi, pp. 571-587, Kluwer Academic Publishers, Dordrecht, 1991.

Richards, M. A., R. A. Duncan, and V. E. Courtillot, Flood basalts and hot spot tracks: Plume heads and tails, *Science, 246*, 103-107, 1989.

Richards, M. A., and R. W. Griffiths, Deflection of plumes by mantle shear flow: experimental results and a simple theory, *Geophys. J., 94*, 367-376, 1988.

Richards, M. A., and R. W. Griffiths, Thermal entrainment by deflected mantle plumes, *Nature, 342*, 900-902, 1989.

Richards, M. A., and B. H. Hager, Geoid anomalies in a dynamic Earth, *J. Geophys. Res., 89*, 5987-6002, 1984.

Richards, M. A., Y. Ricard, C. Lithgow-Bertelloni, G. Spada, and R. Sabadini, An explanation for Earth's long-term rotational stability, *Science, 275*, 372-375, 1997.

Sager, W. W., Paleomagnetism of Abbott Seamount and implications for the latitudinal drift of the Hawaiian hot spot, *J. Geophys. Res., 89*, 6271-6284, 1984.

Sager, W. W., and U. Bleil, Latitudinal shift of Pacific hotspots during the late Cretaceous and early Tertiary, *Nature, 326*, 488-490, 1987.

Schilling, J.-G., Fluxes and excess temperatures of mantle plumes inferred from their interaction with migrating mid-ocean ridges, *Nature, 352*, 397-403, 1991.

Sleep, N., Hotspots and mantle plumes: Some phenomenology, *J. Geophys. Res., 95*, 6715-6736, 1990.

Sleep, N., Time dependence of mantle plumes: Some simple theory, *J. Geophys. Res., 97*, 20007-20019, 1992.

Steinberger, B., Plumes in a convecting mantle: Models and observations for individual hotspots, *J. Geophys. Res.*, in press, 1999.

Steinberger, B., and R. J. O'Connell, Changes of the Earth's rotation axis owing to advection of mantle density heterogeneities, *Nature, 387*, 169-173, 1997.

Steinberger, B., and R. J. O'Connell, Advection of plumes in mantle flow: implications for hotspot motion, mantle viscosity and plume distribution, *Geophys. J. Int., 132*, 412-434, 1998.

Su, W.-J., R. L. Woodward, and A. M. Dziewonski, Degree 12 model of shear velocity heterogeneity in the mantle, *J. Geophys. Res., 99*, 6945-6980, 1994.

Tarduno, J. A., and R. D. Cottrell, Paleomagnetic evidence for motion of the Hawaiian hotspot during formation of the Emperor seamounts, *Earth Planet. Sci. Lett., 153*, 171-180, 1997.

Tarduno, J. A., and J. Gee, Large-scale motion between Pacific and Atlantic hotspots, *Nature, 378*, 477-480, 1995.

Thoraval, C., and M. A. Richards, The geoid constraint in global geodynamics: viscosity structure, mantle heterogeneity models and boundary conditions, *Geophys. J. Int., 131*, 1-8, 1997.

Watts, A. B., J. K. Weissel, R. A. Duncan, and R. L. Larson, Origin of the Louisville Ridge and its relationship to the Eltanin Fracture Zone System, *J. Geophys. Res., 93*, 3051-3077, 1988.

Wessel, P., and W. H. F. Smith, New version of the Generic Mapping Tools released, *Eos Trans. AGU, 76*, 329, 1995.

Whitehead, J. A., Instabilities of fluid conduits in a flowing earth - are plates lubricated by the asthenosphere? *Geophys. J. R. astr. Soc., 70*, 415-433, 1982.

Whitehead, J. A., and D. S. Luther, Dynamics of laboratory diapir and plume models, *J. Geophys. Res., 80*, 705-717, 1975.

Wilson, J. T., A possible origin of the Hawaiian islands, *Can. J. Phys., 41*, 863-870, 1963.

Wolfe, C. J., I. T. Bjarnason, J. C. VanDecar, and S. C. Solomon, Seismic structure of the Iceland mantle plume, *Nature, 385*, 245-247, 1997.

B. Steinberger, Institut für Meteorologie und Geophysik, Johann Wolfgang Goethe-Universität, Feldbergstr. 47, 60323 Frankfurt am Main, Germany. (e-mail: steinber@geophysik.uni-frankfurt.de)

R. J. O'Connell, Department of Earth and Planetary Sciences, Harvard University, 20 Oxford Street, Cambridge, MA 02138. (e-mail: oconnell@geophysics.harvard.edu)